Sens Imaging (2015) 16:4
DOI 10.1007/s11220-015-0106-3

ORIGINAL PAPER

Multi-Focus Image Fusion Based on NSCT and NSST

Altan-Ulzii Moonon · Jianwen Hu

Received: 2 February 2015
© Springer Science+Business Media New York 2015

Abstract In this paper, a multi-focus image fusion algorithm based on the nonsubsampled contourlet transform (NSCT) and the nonsubsampled shearlet transform (NSST) is proposed. The source images are first decomposed by the NSCT and NSST into low frequency coefficients and high frequency coefficients. Then, the average method is used to fuse low frequency coefficient of the NSCT. To obtain more accurate salience measurement, the high frequency coefficients of the NSST and NSCT are combined to measure salience. The high frequency coefficients of the NSCT with larger salience are selected as fused high frequency coefficients. Finally, the fused image is reconstructed by the inverse NSCT. We adopt three metrics ($Q^{AB/F}$, Q_e and Q_w) to evaluate the quality of fused images. The experimental results demonstrate that the proposed method outperforms other methods. It retains highly detailed edges and contours.

Keywords Multi-focus image fusion · Nonsubsampled contourlet transform · Nonsubsampled shearlet transform · Low frequency coefficient · High frequency coefficient

This article is part of the Topical Collection on Hybrid Imaging and Image Fusion.

A.-U. Moonon
College of Electrical and Information Engineering, Hunan University, Changsha 410082, People's Republic of China
e-mail: altanolzii_m@yahoo.com

J. Hu (✉)
College of Electrical and Information Engineering, Changsha University of Science and Technology, Changsha 410114, People's Republic of China
e-mail: hujianwen1@163.com

Published online: 19 February 2015

1 Introduction

In optic systems, a lens can exactly focus on one given distance at a time. Figure 1 illustrates an optic lens model. The optic lens receives the light and projects it onto the sensor, and then the sensor measures the light. In order that light from the object "B" coverage at the same location on the sensor, the object "B" will sharp and "in focus" in image. Besides, the objects "A" and "C" will out focus in image. It is dependent on the depth of field (DOF), which is a region wherein objects appear sharp in the image. The DOF is described by various limitations of technical parameters such as aperture, focal length and circle confusion. Larger aperture and longer focal length (object close to lens) make a larger circle of confusion. Larger circle of confusion, given shallow DOF, means only an object focused in image. Therefore, it is impossible that all objects are in focus when you capture an image at one distance. One way to solve this problem is using multi-focus image fusion. Multi-focus image fusion is the process of combining different focus points of two or more images of a scene, into a single highly informative and everywhere focused image that is more suitable for computer processing and visual perception. Multi-focus image fusion is widely used in medical diagnostics, remote sensing and military applications.

In recent years the commonly used image fusion algorithms are based on multi-scale geometric analysis (MGA) such as contourlet and shearlet [1–3]. The MGA methods can more accurately capture the image edge information and provide higher directional sensitivity than wavelets [4–7]. Do and Vetterli proposed the contourlet transform (CT) in 2002, which can represent image salient features more effectively [1]. In 2006, the NSCT introduced by Cunha et al. [2] discards the downsampling step during image decomposition stage of the contourlet transform. The NSCT is shift invariant versions of contourlet transform. Shift-invariance is very important for image fusion. Therefore the NSCT is more suitable for image fusion.

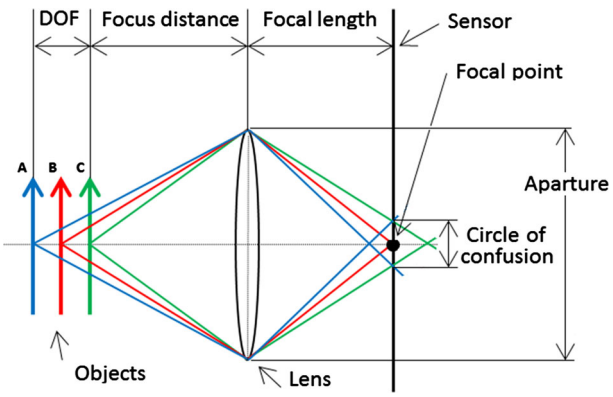

Fig. 1 Optic lens model

The shearlet transform designed by Guo and Labate is one new MGA method [3]. It is expected to obtain a two-dimensional affine system for exhibiting the geometric and mathematical properties of images, e.g., directionally, elongated shapes, scales and oscillation [3]. Miao et al. suggested that the shearlet transform presents good fusion performance, but the lack of shift invariance cannot be ignored [8]. Easley et al. proposed the nonsubsampled shearlet transform, which combines the nonsubsampled Laplacian pyramid transform with several different shearing filters [9]. In other words, the NSST is a shift invariant version of the shearlet transform.

After considering the advantages of the NSST and NSCT, we propose a new image fusion method by combining the NSCT and NSST in this paper. The remainder of the paper is structured as follows: In Sect. 2, we briefly review the NSCT and NSST. The proposed algorithm is presented in Sect. 3. The experimental results and analysis are given in Sect. 4, and the paper is concluded in Sect. 5.

2 NSCT and NSST

The NSCT and NSST are two new multi-scale geometrical analysis methods. In this section, we will briefly review the NSCT and NSST, which can decompose source images into a low frequency sub-band and several high frequency sub-bands with different directions.

2.1 Nonsubsampled Contourlet Transform

The NSCT is a shift invariant version of the CT. The NSCT is built by the nonsubsampled pyramid (NSP) and the nonsubsampled directional filter bank (NSDFB). The NSP is the multi-scale property of the NSCT. It is obtained from a shift-invariant filtering structure. The subband decomposition of the NSP is similar to the Laplacian pyramid which is achieved by using two channel nonsubsampled 2-D filter banks. The NSP developed from *à trous* algorithm. The tree structure and shift-invariant directional expansion of the NSCT are obtained from the nonsubsampled directional filter bank (NSDFB), which is constructed by eliminating the down sampler and up sampler in the directional filter bank (DFB). The DFB is constructed by combining critically sampled fan filter banks and re-sampling operations [2]. All filter banks in the NSDFB tree structure are obtained from a single nonsubsampled filter bank (NSFB) with fan filter. It decomposes high frequency sub-band into several directional sub-bands.

The structure of the NSCT is illustrated in Fig. 2a. Figure 2b illustrates the corresponding frequency division of the NSCT, where the number of directions is increased with frequency [2]. The NSCT is flexible in that it allows any number of 2^{l} directions in each scale, where l is a positive integer. If the numbers of directions in the NSDFB expansion are doubled at every other scale, the NSCT can satisfy anisotropic scaling law that is a key property in establishing the expansion nonlinear approximation behaviour. The NSCT has redundancy given by one lowpass frequency sub-band and $\sum_{j=1}^{J} 2^{lj}$ high frequency sub-band, where lj denotes the number of levels in the NSDFB at the jth scale.

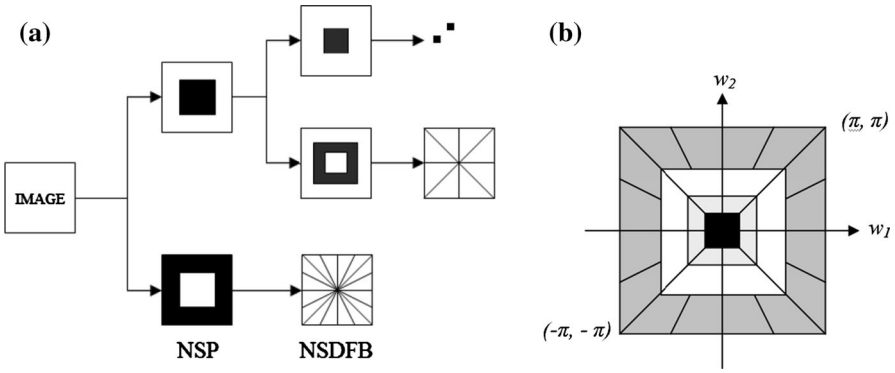

Fig. 2 The nonsubsampled contourlet transform. **a** Structure of the NSCT. **b** Correspond frequency division of the NSCT

2.2 Nonsubsampled Shearlet Transform

For a continuous wavelet $\psi \in L^2(\mathbb{R}^2)$, consider the two-dimensional affine system

$$\left\{\psi_{ast}(x) = |\det M_{as}|^{\frac{1}{2}}\psi\left(M_{as}^{-1}x - t\right) : t \in \mathbb{R}^2, M_{as} \in \Gamma\right\} \tag{1}$$

where Γ is the 2 parameter dilation group

$$\Gamma = \left\{M_{as} = \begin{pmatrix} a & \sqrt{a}s \\ 0 & \sqrt{a} \end{pmatrix} : (a,s) \in \mathbb{R}^+ \times \mathbb{R}\right\} \tag{2}$$

For any row vectors $\xi = (\xi_1, \xi_2) \in \hat{\mathbb{R}}^2,\ \xi_1 \neq 0\,\psi$ is that:

$$\hat{\psi}(\xi) = \hat{\psi}(\xi_1, \xi_2) = \hat{\psi}_1(\xi_1)\hat{\psi}_2\left(\frac{\xi_2}{\xi_1}\right) \tag{3}$$

where continuous wavelets $\hat{\psi}_1, \hat{\psi}_2 \in C^\infty(\mathbb{R})$. According to the Eq. (3), ψ is a continuous wavelet and for $a \in \mathbb{R}^+$, $s \in \mathbb{R}$ and $a \in \mathbb{R}^2$

$$Sf(a,s,t) = <f, \psi_{ast}> \tag{4}$$

Equation (4) is called continuous shearlet transform of $f \in L^2(\mathbb{R})$ [9, 10]. The discrete shearlet transform $\hat{\psi}_{jlk}\left(j \geq 0, -2^j \leq l \leq 2^j - 1, k \in \mathbb{Z}^2\right)$, which can deal with distributed discontinuities, is obtained by sampling continuous shearlet transform *Sf*(*a*, *s*, *t*) [3]. Each element of $\hat{\psi}_{jlk}$ supported on a pair of trapezoids of approximate size $2^{2j} \times 2^j$. This is illustrated on Fig. 3a. In Fig. 3b illustrated tilling of frequency plane that it is induced by shearlet transform.

One important advantage of the shearlet transform is that there are no restrictions on the number of directions for the shearing [11]. Also, in the shearlet, there are no constraints on the size of the supports for the shearing, unlike the construction of the directional filter banks in [9]. The NSST consists of two phases, which are the non-

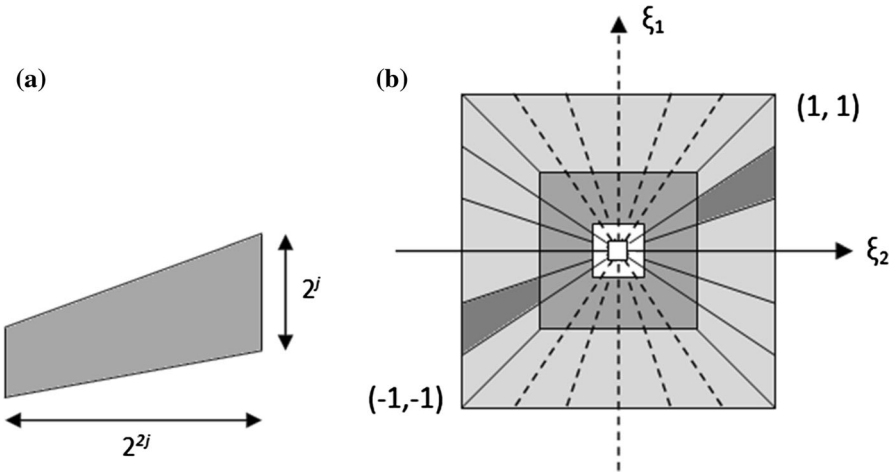

Fig. 3 **a** The frequency support of a shearlet $\hat{\psi}_{jlk}$ satisfies parabolic scaling. **b** The tilling of frequency plane induced by shearlet

subsampled Laplacian pyramid and several different combinations of shearing filters [3]. The NSST is not only shift–invariant, but also multi-scale and exhibits multi-directional expansion.

3 Combined Algorithm of NSCT and NSST

The block diagram of the proposed method is shown in Fig. 4. The detailed steps are presented as follows:

Step 1: Decompose the source images into a pair of low frequency coefficients $\{L^A_{nsct}, L^B_{nsct}\}$, $\{L^A_{nsst}, L^B_{nsst}\}$ and high frequency coefficients $\left\{H^{(s,d)}_{nsct}, H^{(s,d)}_{nsct}\right\}$, $\left\{H^{(s,d)}_{nsst}, H^{(s,d)}_{nsst}\right\}$ via the NSCT and NSST, respectively. Where s is the number of multi-scale decomposition levels and d is direction of decomposition at the s-th level.

Step 2: Take the average of low frequency coefficients of the NSCT to get the low frequency fusion coefficient.

$$L_F = \frac{1}{2}\left(L^A_{nsct} + L^B_{nsct}\right) \tag{5}$$

where L^A_{nsct} and L^B_{nsct} are low frequency coefficients of the NSCT, L_F is the fused low frequency coefficient.

Step 3: According to the following method, the high frequency coefficients of the NSCT and NSST are combined to obtain the fused high frequency coefficients of the NSCT.

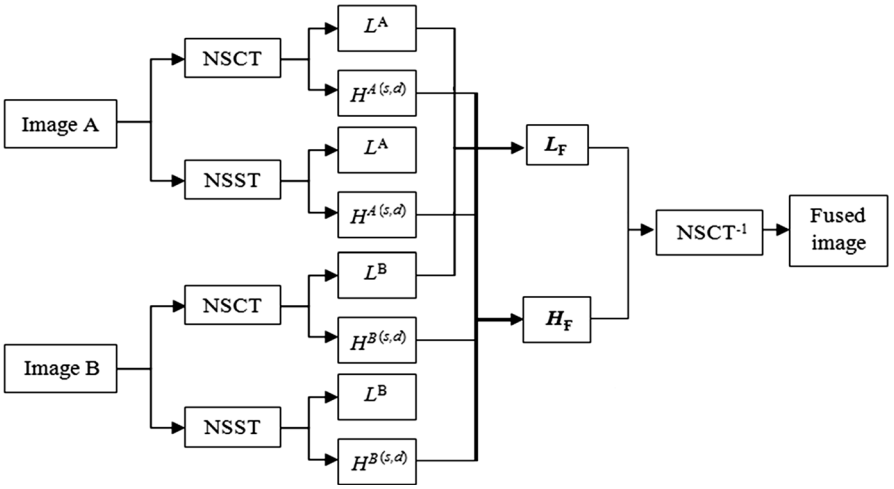

Fig. 4 Block diagram of the proposed method

- Firstly, compute the energy of each patch (region energy) around each pixel for each of the high frequency coefficients. The advantage of using region energy can reduce influence of noise in the fused image.

$$RE^{(s,d)}(i,j) = \sum_{m=-M}^{M} \sum_{n=-M}^{M} \left(H^{(s,d)}(i+m, j+n) \right)^2 \tag{6}$$

where $H^{(s,d)}$ is d-th direction of s-th level high frequency coefficient of the NSCT and NSST for each image. M is set as 3.

- Secondly, use region energy coefficient to calculate the salience of high frequency coefficients by combining the NSCT and NSST in d-th direction of s-th level for each image.

$$X^{(s,d)}(i,j) = \sqrt{\left(RE_{nsct}^{(s,d)}(i,j) \right)^2 + \left(RE_{nsst}^{(s,d)}(i,j) \right)^2} \tag{7}$$

where $RE_{nsct}^{(s,d)}$ and $RE_{nsst}^{(s,d)}$ are the region energy coefficient of the NSCT and NSST respectively, i and j are pixel position of source image. $X^{(s,d)}$ is the salience of high frequency coefficients of the NSCT, which reflects the definition of source images. Larger $X^{(s,d)}$ indicates more clear images.

- Then, we choose high frequency coefficients with larger $X^{(s,d)}$ as the fused high frequency coefficients.

$$H_F^{(s,d)}(i,j) = \begin{cases} H_{nsct}^{A(s,d)}(i,j) \; X_{\mathrm{A}}^{(s,d)}(i,j) \geq X_{\mathrm{B}}^{(s,d)}(i,j) \\ H_{nsct}^{B(s,d)}(i,j) \; \text{otherwise} \end{cases} \tag{8}$$

where $H_F^{(s,d)}$ is the high frequency fusion coefficient.

Step 4: Obtain fused image from fused low and high frequency coefficients via the inverse the NSCT.

4 Experimental Results and Analysis

In this section, the performance of the proposed method is tested and compared against the image fusion methods based on individual NSCT, NSST and the NSCT-SF-PCNN by objective evaluation and visual inspection. The NSCT-SF-PCNN is one of state-of-the-art fusion algorithms proposed by Qu et al. [12]. The Eqs. (5) and (6) based choose-abs-max fusion rule used to fuse low and high frequency coefficient of the NSCT and NSST, respectively. Experiments were performed with MATLAB 8.1 (64bit) on i5 2.3 GHz CPU, 4 GB of RAM laptop. Shearlet, NSCT and NSCT-SF-PCNN toolboxes are used for experiments. Five pairs of multi-focus images as seen in Fig. 5a–j are used to test the performance of our method.

We adopt three metrics ($Q^{AB/F}$, Q_e and Q_w) to evaluate the quality of fused images [13, 14]. The metric $Q^{AB/F}$ evaluates the quality of visual information obtained from source images. Both the metric Q_w and Q_e evaluate the structural similarity between fused image and source images. The metric Q_w considers the local salience, and the metric Q_e integrates the importance of edge. The values of all metrics are between 0 and 1. If their values are near to 1, fusion results indicate better quality.

The decomposition of the NSCT and NSST is based on Laplacian pyramid filtering and directional filtering. Firstly, we analysed the influence of different pyramid and directional filters to the performance of the proposed method. For this analysis we considered various types of pyramid filters for the NSCT and NSST, namely *pyr* (derived from 1-D filters using maximally flat mapping function with 2 vanishing moments), *pyrexc* (same with *pyr*, but with two highpass filters

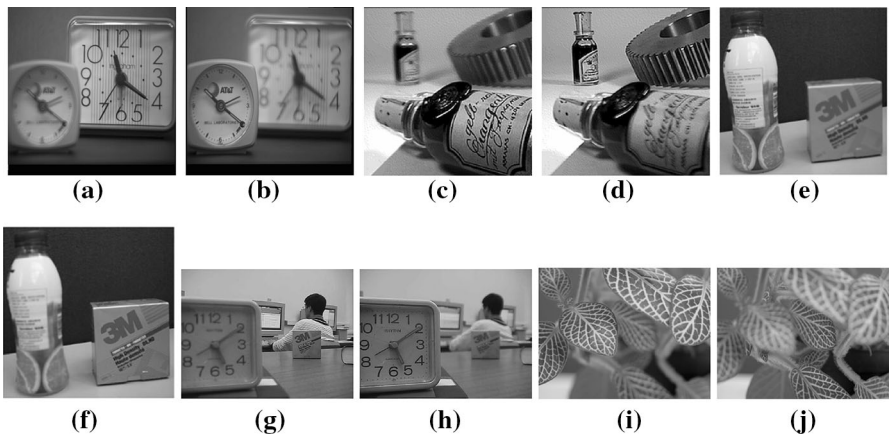

Fig. 5 Five pairs of multi-focus test images

exchanged), *maxflat* (derived from 1-D filters using maximally flat mapping function with 4 vanishing moments) and 9–7 (derived from 9 to 7 1-D prototypes) while a type of directional filter for NSCT, namely *cd* (derived from 9 to 7 biorthogonal filters using McClellan transformed by Cohen and Daubechies), *pkva* (ladder filters by Phong et al.) and *vk* (McClellan transformed of the filter from the VK book).

The decomposition level of the NSCT is set as {4, 8, 8, 16}. In the NSST, there is no directional filter bank, unlike the NSCT. There are shearing window works for directional potential. If we use only the NSST for multifocus image fusion, higher number of shearing directions provides better fusion result. But in our case, when shearing directions number is lower, the proposed method provides better results. Due to a number of experiments, we chose shearing directions number {4 6 6 8}, it provides better results for Table 1 and all other experiments. The best results are labeled by bold in all tables. Table 1 gives the results of four different combinations of the filters, and it shows that the combination of the filters *pyrexc* & *cd* for the NSCT and the pyramid filter *maxflat* for the NSST is better than the other three combination filters.

In Table 2, we show test result of the proposed method using the inverse the NSST to obtain fused image. The list presents that the results of combination filters *pyr* & *cd* and *pyr* are better than others. On the whole, the inverse the NSCT obtain better results than the inverse the NSST. Accordingly, with the comparisons between Tables 1 and 2, the combination of filters *pyrexc* & *cd* for the NSCT and pyramid filter *maxflat* for the NSST is selected. The next experiment is to analyse the influence of different decomposition levels for the proposed method. For this testing, we set as the filters *pyrexc* & *cd* for the NSCT, filter *maxflat* for the NSST and number shearing directions set as {4, 6, 6, 8}. For the decomposition level setting, we test ten different decomposition level options.

To save space, we choose only three different decomposition levels, and the results are shown in Table 3. The bolded values are the best results. The result shows that the decomposition level {4, 8, 8, 16} and {8, 8, 8, 16} are better than other decomposition level option. Few decomposition levels can reduce time consumption. Therefore we set decomposition level as {4, 8, 8, 16} for the proposed method.

We performed the number of experiments for influence of directional filters on the proposed method. The experimental results are listed in Table 4. As a consequence *cd* filter provides better results for each testing images of Fig. 5. Therefore we chose *cd* filter for the proposed method.

The proposed method is compared with individual NSCT, NSST and the NSCT-SF-PCNN. For the individual NSCT and NSST, according to the result of parameters setting test, we choose the best parameter set. For the NSCT of the proposed method, the number of directions from coarser to finer scale is set to {4, 8, 8, 16}, and the pyramid filter and the directional filter are set to *pyrexc* and *cd* respectively. In the NSST, it sets as {4, 8, 8, 16} directions with *pyrexc* for pyramid filter when number of shearing directions set as {4, 6, 6, 8}. The NSCT-SF-PCNN parameter option is that the NSCT settings same with individual NSCT and PCNN settings are default option by [12]. The comparison results of different fusion

Table 1 Comparison result of different filter combination

Metrics	Pyramid and directional filters of NSCT	Pyramid filters of NSST	Figure 5a, b (512 × 512)	Figure 5c, d (192 × 192)	Figure 5e, f (256 × 256)	Figure 5g, h (640 × 480)	Figure 5i, j (270 × 205)
$Q^{AB/F}$	pyrexc & cd	maxflat	0.6912	**0.7343**	**0.7979**	**0.7279**	0.7219
	pyr & cd	maxflat	**0.6921**	0.7342	0.7962	**0.7279**	0.7225
	pyrexc & cd	9–7	0.6914	0.7341	0.7976	0.7272	0.7222
	pyr & cd	9–7	0.6919	0.7342	0.7963	**0.7279**	**0.7227**
Q_w	pyrexc & cd	maxflat	0.8928	**0.8977**	**0.9389**	0.8884	**0.9013**
	pyr & cd	maxflat	**0.8930**	0.8975	0.9386	0.8884	**0.9013**
	pyrexc & cd	9–7	0.8927	0.8976	**0.9389**	0.8884	**0.9013**
	pyr & cd	9–7	0.8929	0.8975	0.9387	**0.8885**	**0.9013**
Q_e	pyrexc & cd	maxflat	0.7483	**0.7919**	**0.8769**	0.8095	0.8129
	pyr & cd	maxflat	**0.7485**	0.7918	0.8747	0.8096	0.8129
	pyrexc & cd	9–7	0.7481	0.7918	**0.8768**	0.8096	**0.8130**
	pyr & cd	9–7	0.7484	0.7917	0.8749	**0.8097**	**0.8130**

Table 2 Comparison result of different filter combination when fused image reconstructed by inverse the NSST

Metrics	Pyramid and directional filters of NSCT	Pyramid filters of NSST	Figure 5a, b (512 × 512)	Figure 5c, d (192 × 192)	Figure 5e, f (256 × 256)	Figure 5g, h (640 × 480)	Figure 5i, j (270 × 205)
$Q^{AB/F}$	pyrexc & cd	pyrexc	0.6913	0.7338	0.7901	0.7263	0.7223
	pyr & cd	pyr	**0.6922**	**0.7342**	**0.7914**	0.7271	0.7230
	pyrexc & cd	9–7	0.6921	0.7340	0.7897	**0.7283**	**0.7240**
	pyr & cd	9–7	0.6919	0.7341	0.7892	**0.7285**	**0.7240**
Q_w	pyrexc & cd	pyrexc	**0.8918**	**0.8975**	**0.9295**	0.8883	**0.9014**
	pyr & cd	pyr	**0.8918**	0.8973	**0.9295**	**0.8884**	**0.9014**
	pyrexc & cd	9–7	0.8910	0.8965	0.9367	0.8882	0.9010
	pyr & cd	9–7	0.8908	0.8964	0.9366	0.8882	0.9010
Q_e	pyrexc & cd	pyrexc	0.7486	**0.7914**	**0.8508**	0.8093	**0.8131**
	pyr & cd	pyr	**0.7487**	0.7912	0.8504	**0.8096**	**0.8131**
	pyrexc & cd	9–7	0.7474	0.7899	0.8692	0.8093	0.8126
	pyr & cd	9–7	0.7469	0.7899	0.8691	0.8093	0.8125

Table 3 Comparison result of decomposition level for the proposed method

Metrics	Decomposition level of NSCT and NSST	Figure 5a, b (512 × 512)	Figure 5c, d (192 × 192)	Figure 5e, f (256 × 256)	Figure 5g, h (640 × 480)	Figure 5i, j (270 × 205)
$Q^{AB/F}$	4 4 8 16	0.6896	0.7325	0.7883	**0.7270**	0.7216
	4 8 8 16	**0.6900**	**0.7326**	0.7879	0.7269	0.7215
	8 8 8 16	**0.6900**	**0.7326**	**0.7890**	0.7268	**0.7219**
Q_w	4 4 8 16	**0.8914**	0.8969	0.9309	**0.8882**	0.9010
	4 8 8 16	0.8912	**0.8970**	**0.9311**	**0.8882**	**0.9012**
	8 8 8 16	0.8913	**0.8970**	**0.9311**	**0.8882**	**0.9012**
Q_e	4 4 8 16	**0.7483**	0.7902	0.8544	0.8089	0.8124
	4 8 8 16	0.7477	**0.7903**	**0.8551**	**0.8090**	0.8125
	8 8 8 16	0.7477	**0.7903**	**0.8551**	**0.8090**	**0.8126**

Table 4 Comparison result of different directional filters of the NSCT for the proposed method

Metrics	Directional filters of NSCT	Figure 5a, b (512 × 512)	Figure 5c, d (192 × 192)	Figure 5e, f (256 × 256)	Figure 5g, h (640 × 480)	Figure 5i, j (270 × 205)
$Q^{AB/F}$	cd	**0.6912**	**0.7343**	**0.7979**	**0.7274**	**0.7219**
	vk	0.6908	0.7332	0.7957	0.7259	0.7186
	pkva	0.6811	0.7303	0.7927	0.7199	0.7149
Q_w	cd	**0.8928**	**0.8978**	**0.9389**	**0.8888**	**0.9013**
	vk	0.8924	0.8978	0.9385	0.8887	0.9012
	pkva	0.8915	0.8964	0.9388	0.8881	0.9014
Q_e	cd	**0.7483**	0.7919	0.8769	**0.8099**	**0.8129**
	vk	0.7477	**0.7920**	0.8757	0.8098	0.8124
	pkva	0.7478	0.7896	**0.8780**	0.8089	0.8125

Table 5 Comparison result of different fusion methods

Metrics	Methods	Figure 5a, b (512 × 512)	Figure 5c, d (192 × 192)	Figure 5e, f (256 × 256)	Figure 5g, h (640 × 480)	Figure 5i, j (270 × 205)
$Q^{AB/F}$	NSCT	0.6876	0.7314	0.7948	0.7214	0.7146
	NSST	0.6830	0.7298	0.7917	0.7204	0.7132
	NSST-SF-PCNN	0.6902	0.7229	0.7901	0.7171	0.7056
	Proposed	**0.6912**	**0.7343**	**0.7979**	**0.7274**	**0.7219**
Q_w	NSCT	0.8919	**0.8977**	**0.9393**	**0.8884**	0.9010
	NSST	0.8921	0.8973	0.9298	**0.8884**	0.9010
	NSST-SF-PCNN	0.8739	0.8863	0.9281	0.8655	0.8894
	Proposed	**0.8928**	**0.8977**	0.9389	**0.8884**	**0.9013**
Q_e	NSCT	**0.7483**	0.7917	**0.8784**	0.8090	0.8112
	NSST	0.7482	0.7916	0.8514	0.8092	0.8114
	NSST-SF-PCNN	0.6916	0.7654	0.8502	0.7692	0.7846
	Proposed	**0.7483**	**0.7919**	0.8769	**0.8095**	**0.8129**

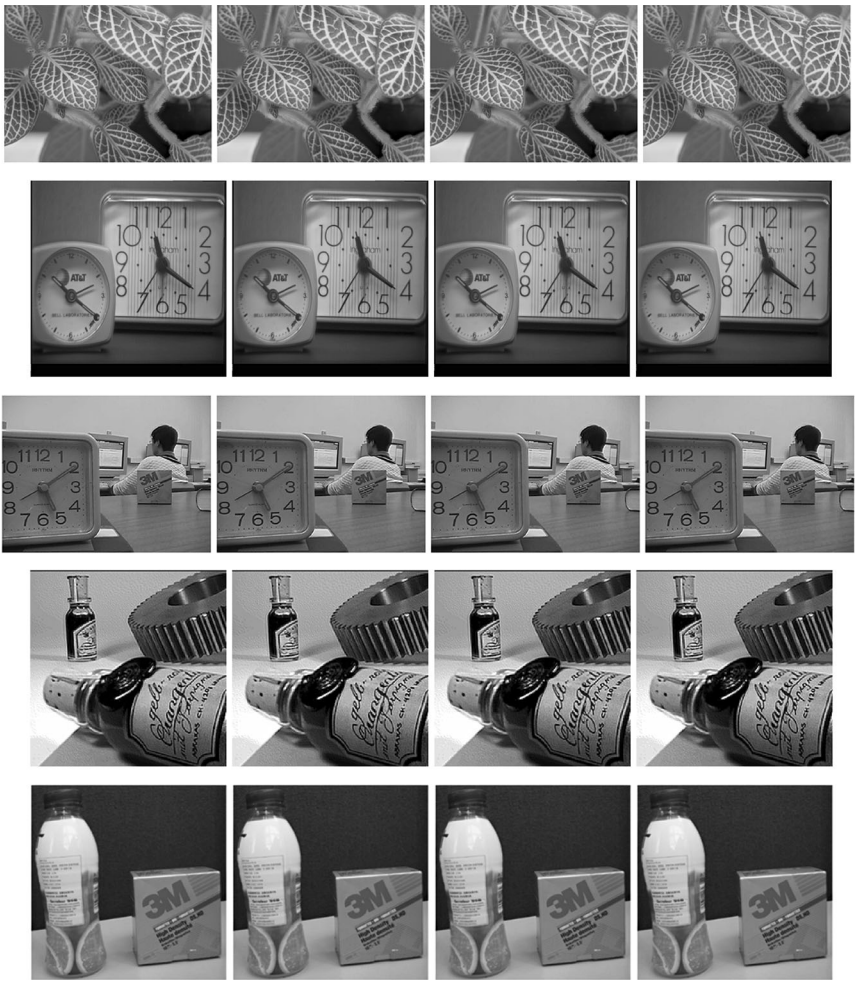

Fig. 6 The image fusion results. The *first column* is the result of the NSCT, the *second column* is the result of the NSST, the *third column* is the result of the NSCT-SF-PCNN and the *last column* shows the results of the proposed method

methods are shown in Table 5 and Fig. 6. The column 1, 2, 3 and 4 of Fig. 6 are fusion results of the NSCT, NSCT, NSCT-SF-PCNN and the proposed method, respectively. Visual performance of Fig. 6 is good for all methods. Table 5 illustrates that the proposed method achieves higher values than those compared method.

To further test the performance of the proposed method, we performed experiments over multi-focus colour images. Each band of colour image is separately fused by the proposed algorithm. All parameter settings are the same as in the previous experimental options. Figure 7 and Table 6 show the experimental results. All the fused images Fig. 7e–h and i–l are good by the visual inspection. In

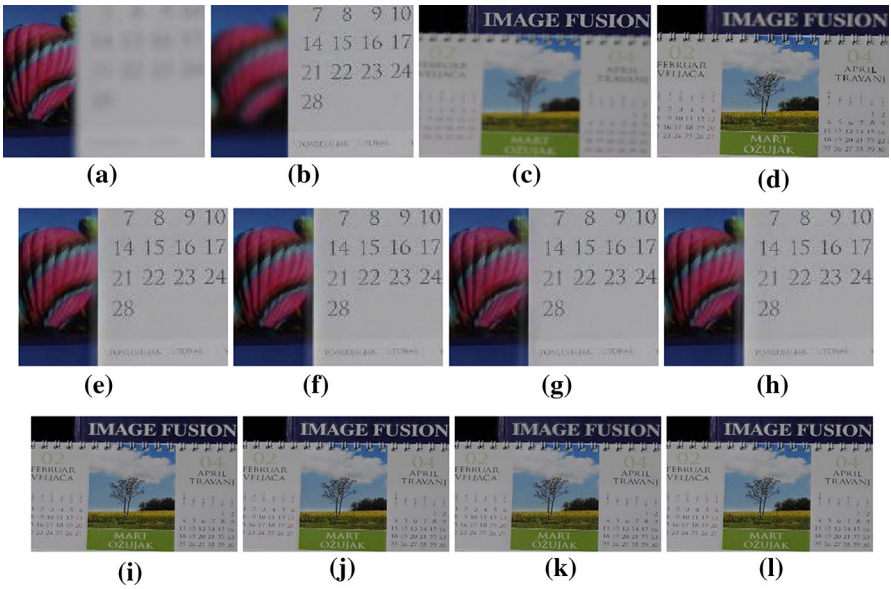

Fig. 7 Multi-focus colour image fusion results. **a**–**d** are source images. **e** and **i** are results of the NSCT, **f** and **j** are results of the NSST, **g** and **k** are results of the NSCT-SF-PCNN, **h** and **l** are results of the proposed method

Table 6 Comparison results of multi-focus colour image fusion methods

Metrics	Methods	Figure 7a, b (178 × 134)				Figure 7d, e (267 × 175)			
		Red	Green	Blue	Average	Red	Green	Blue	Average
$Q^{AB/F}$	NSCT	0.7202	0.7349	0.7359	0.7303	0.6944	0.6940	0.6953	0.6946
	NSST	0.7266	0.7351	0.7384	0.7334	0.6979	0.6994	0.7006	0.6993
	NSCT-SF-PCNN	0.7203	0.7404	0.7375	0.7327	0.6987	0.6986	0.7013	0.6995
	Proposed method	**0.7297**	**0.7534**	**0.7431**	**0.7421**	**0.7018**	**0.7035**	**0.7036**	**0.7030**
Q_w	NSCT	0.9468	0.9506	0.9528	0.9501	0.9204	0.9214	0.9170	0.9196
	NSST	0.9474	0.9511	0.9531	0.9505	0.9200	0.9210	0.9166	0.9192
	NSCT-SF-PCNN	0.9422	0.9472	0.9489	0.9461	0.9193	0.9205	0.9149	0.9182
	Proposed method	**0.9484**	**0.9526**	**0.9538**	**0.9516**	**0.9212**	**0.9222**	**0.9176**	**0.9203**
Q_e	NSCT	0.9126	0.9213	0.9236	0.9192	0.8324	0.8340	0.8269	0.8311
	NSST	0.9136	0.9219	0.9239	0.9198	0.8316	0.8333	0.8260	0.8303
	NSCT-SF-PCNN	0.9077	0.9186	0.9201	0.9155	0.8208	0.8216	0.8180	0.8201
	Proposed method	**0.9138**	**0.9233**	**0.9246**	**0.9206**	**0.8333**	**0.8349**	**0.8276**	**0.8319**

Table 7 Time consumption result of different fusion methods

Methods	Figure 5a, b (512 × 512)	Figure 5c, d (192 × 192)	Figure 5e, f (256 × 256)	Figure 5g, h (640 × 480)	Figure 5i, j (270 × 205)	Figure 7a, b (178 × 134)	Figure 7d, e (267 × 175)
NSCT	47.7235 s	6.0247 s	10.7334 s	54.5095 s	9.4083 s	3.2052	6.1286
NSST	19.3069 s	2.6701 s	4.1698 s	27.1523 s	5.7165 s	2.1819	3.7338
NSST-SF-PCNN	174.5254 s	22.6902 s	40.9332 s	204.1247 s	34.9542 s	46.1752	100.8514
Proposed	68.1781 s	9.2564 s	15.7029 s	93.8497 s	16.3334 s	5.2975	9.1802

the results of Table 6, all metrics of the proposed method are better than other three methods. Therefore, the proposed method presents better performance in terms of both visual inspection and objective evaluation.

In Table 7 we show the time consumption of the four fusion methods. Table 7 indicates that the proposed method is slower than individual NSCT, NSST methods and faster than NSCT-SF-PCNN method. However, it should be not an obstacle with the rapid development of hardware and parallel computing technology.

5 Conclusions

In this paper, we proposed a new fusion method based on the NSCT and NSST for multi-focus images. The experimental results demonstrate that our method outperforms individual NSCT, NSST and the NSCT-SF-PCNN, and preserves more edge and contour information. We will focus on using the proposed method to study on other areas of image processing such as image denoising and image enhancement.

Acknowledgments The authors would like to thank the editor and anonymous reviewers for their detailed review and valuable comments. This paper is supported by scientific Research Fund of Hunan Provincial Education Department (No. 14B006).

References

1. Do, M. N., & Vetterli, M. (2005). The contourlet transform: an efficient directional multiresolution image representation. *IEEE Transactions on Image Processing, 14*(12), 2091–2106.
2. Cunha, A. L., Zhou, J., & Do, M. N. (2006). The nonsubsampled contourlet transform: theory, design, and applications. *IEEE Transactions on Image Processing, 15*(10), 3089–3101.
3. Guo, K., & Labate, D. (2007). Optimally sparse multidimensional representation using shearlets. *SIAM Journal on Mathematical Analysis, 39*(1), 298–318.
4. Yang, B., Li, S. T., & Sun, F. M. (2007). Image fusion using nonsubsampled contourlet transform. *Proceedings of the Fourth International Conference on Image and Graphics*, pp. 719–724.
5. Krishnamoorthy, S., & Soman, K. P. (2010). Implementation and comparative study of image fusion. *International Journal of Computer Applications, 9*(2), 25–35.
6. Manu, V. T., & Simon, P. (2012). A novel statistical fusion rule for image fusion and its comparison in non subsampled contourlet transform domain and wavelet domain. *The International Journal of Multimedia and Its Applications, 4*(2), 69–87.
7. Miao, Q. G., Lou, J. J., & Xu, P. F. (2012). Image fusion based on NSCT and bandelet transform. *Proceedings of the Eighth International Conference on Computational Intelligence and Security*, pp. 314–317.
8. Miao, Q. G., Shi, C., Xu, P. F., Yang, M., & Shi, Y. B. (2011). Multi-focus image fusion algorithm based on shearlets. *Chinese Optics Letters, 9*(4), 041001–04005.
9. Easley, G., Labate, D., & Lim, W. Q. (2008). Sparse directional image representations using the discrete shearlet transform. *Applied and Computational Harmonic Analysis, 25*(1), 25–46.
10. Guo, K., Labate, D., & Lim, W. Q. (2009). Edge analysis and identification using the continuous shearlet transform. *Applied and Computational Harmonic Analysis, 27*(1), 24–46.
11. Cao, Y., Li, S. T., & Hu, J. W. (2011). Multi-focus image fusion by nonsubsampled shearlet transform. *Sixth International Conference on Image and Graphics*, pp. 17–21.
12. Qu, X. B., Yan, J. W., Xiao, H. Z., & Zhu, Z. Q. (2009). Image fusion algorithm based on spatial frequency-motivated pulse coupled neural networks in nonsubsampled contourlet transform domain. *Acta Automatica Sinica, 34*(12), 1508–1514.

13. Xydeas, C. S., & Petrovic, V. (2000). Objective image fusion performance measure. *Electronics Letters, 36*(4), 308–309.
14. Piella, G., & Heijmans, H. (2003). A new quality metric for image fusion. *International Conference on Image Processing, 3*, 173–176.